

Strong field ionization of molecules on the surface of nanosystems

Qiwen Qu(曲棋文), Fenghao Sun(孙烽豪), Jiawei Wang(王佳伟), Jian Gao(高健), Hui Li(李辉), and Jian Wu(吴健)

Citation: Chin. Phys. B, 2024, 33 (**4**): 047803. DOI: 10.1088/1674-1056/ad2509
Journal homepage: http://cpb.iphy.ac.cn; http://iopscience.iop.org/cpb

What follows is a list of articles you may be interested in

Gamma induced changes in Makrofol/CdSe nanocomposite films

Ali A. Alhazime, M. ME. Barakat, Radiyah A. Bahareth, E. M. Mahrous,Saad Aldawood, S. Abd El Aal, and S. A. Nouh

Chin. Phys. B, 2022, 31 (**9**): 097802. DOI: 10.1088/1674-1056/ac4909

Quantitative evaluation of LAL productivity of colloidal nanomaterials: Which laser pulse width is more productive, ergonomic, and economic?

Alena Nastulyavichus, Nikita Smirnov, and Sergey Kudryashov

Chin. Phys. B, 2022, 31 (**7**): 077803. DOI: 10.1088/1674-1056/ac5602

Strong near-field couplings of anapole modes and formation of higher-order electromagnetic modes in stacked all-dielectric nanodisks

Bin Liu(刘彬), Ma-Long Hu(胡马龙), Yi-Wen Zhang(章艺文), Yue You(游悦), Zhao-Guo Liang(梁钊国), Xiao-Niu Peng(彭小牛), and Zhong-Jian Yang(杨中见)

Chin. Phys. B, 2022, 31 (**5**): 057802. DOI: 10.1088/1674-1056/ac3bac

Improving the performance of a GaAs nanowire photodetector using surface plasmon polaritons

Xiaotian Zhu(朱笑天), Bingheng Meng(孟兵恒), Dengkui Wang(王登魁), Xue Chen(陈雪), Lei Liao(廖蕾), Mingming Jiang(姜明明), and Zhipeng Wei(魏志鹏)

Chin. Phys. B, 2022, 31 (**4**): 047801. DOI: 10.1088/1674-1056/ac1e15

Effect of local environment in resonant domains of polydisperse plasmonic nanoparticle aggregates on optodynamic processes in pulsed laser fields

A. E. Ershov, A. P. Gavrilyuk, S. V. Karpov, P. N. Semina

Chin. Phys. B, 2015, 24 (**4**): 047804. DOI: 10.1088/1674-1056/24/4/047804

TOPICAL REVIEW — Optical field manipulation

Strong field ionization of molecules on the surface of nanosystems

Qiwen Qu(曲棋文)[1], Fenghao Sun(孙烽豪)[1], Jiawei Wang(王佳伟)[1], Jian Gao(高健)[1,2], Hui Li(李辉)[1,†], and Jian Wu(吴健)[1,2,3,4]

[1] *State Key Laboratory of Precision Spectroscopy, East China Normal University, Shanghai* 200241, *China*
[2] *Chongqing Key Laboratory of Precision Optics, Chongqing Institute of East China Normal University, Chongqing* 401121, *China*
[3] *Collaborative Innovation Center of Extreme Optics, Shanxi University, Taiyuan* 030006, *China*
[4] *CAS Center for Excellence in Ultra-Intense Laser Science, Shanghai* 201800, *China*

(Received 27 December 2023; revised manuscript received 25 January 2024; accepted manuscript online 2 February 2024)

Besides the diverse investigations on the interactions between intense laser fields and molecular systems, extensive research has been recently dedicated to exploring the response of nanosystems excited by well-tailored femtosecond laser fields. Due to the fact that nanostructures hold peculiar effects when illuminated by laser pulses, the underlying mechanisms and the corresponding potential applications can make significant improvements in both fundamental research and development of novel techniques. In this review, we provide a summarization of the strong field ionization occurring on the surface of nanosystems. The molecules attached to the nanoparticle surface perform as the precursor in the ionization and excitation of the whole nanosystem, the fundamental processes of which are yet to be discovered. We discuss the influence on nanoparticle constituents, geometric shapes and sizes, as well as the specific waveforms of the excitation laser fields. The intriguing characteristics observed in surface ion emission reflect how enhanced near field affects the localized ionizations and nanoplasma expansions, thereby paving the way for further precision controls on the light-and-matter interactions in the extreme spatial temporal levels.

Keywords: nanoparticle, femtosecond laser field, local field enhancement

PACS: 78.67.Bf, 82.53.Xa, 79.60.Bm, 52.20.Hv **DOI:** 10.1088/1674-1056/ad2509

1. Introduction

In the field of strong-field physics, extensive research has been conducted to investigate the ionization dynamics in atomic and molecular systems when interacting with intense laser fields.[1–7] The exploration of strong-field physics beyond the atomic and molecular systems, e.g., in nanosystems, has garnered significant attention as it holds great potential for advancements in nanoelectronics and nanoionics.[8–11] The reduced size of nanostructures compared to the wavelength of the laser fields leads to a highly enhanced near-field which can induce an increase in localized ionization yield. Electrons and ions produced from the ionized surface molecules attached to the nanosystems might significantly influence the succeeding excitation of the whole nanosystems. Therefore the surface ionization processes play crucial roles. Factors such as material compositions, geometric shapes, particle sizes, together with the incident laser field waveforms determine both near-field properties and the complex ionization processes. By investigating the electron photoemission from isolated nanoparticles of various materials interacting with few-cycle laser pulses, people have observed that the acceleration process of electrons can be significantly influenced by the ionized electrons and residual ions. However, at sufficiently high near-field intensities, the dependence on the material constituents is suppressed due to interactions among many charged particles.[13] Recent research has unveiled an ultrafast metallization process occurring in dielectric nanoparticles. This discovery manifests as a characteristic modification towards metallic limit when the excitation intensities achieve the level of igniting carrier avalanching within the particle volume.[14] The energies of photoelectrons emitted from isolated dielectric nanoparticles exhibit a significant size dependency, with higher energetic electrons for larger nanoparticles. The maximum energies can go up to ~ 200 times the ponderomotive energy due to the dramatic ionization and charge interactions in nanosystems.[17] The enhanced cutoff energies hold great potential for producing attosecond electron bunches through near-field induced photoelectron emission.[11,13,16]

Although poses a challenge to ascertain the origins of electrons, the distinguishing of ion species opens up possibilities for further investigations into the ionization processes occurring on the surface of nanosystems. The surface molecular ionization processes in isolated dielectric nanoparticles have been comprehensively investigated, elucidating the localization of the incident laser field resulting from size effects.[12] Such localized field significantly impacts the probability of proton emission. Besides the characteristics observed in isolated single nanoparticles, the dimer systems composed of

†Corresponding author. E-mail: hli@lps.ecnu.edu.cn

© 2024 Chinese Physical Society and IOP Publishing Ltd

a couple of nanoparticles can produce a more pronounced near field enhancement when interacting with femtosecond laser fields, leading to the generation of distinct distributions in the proton emission at relatively low incident laser intensities.[24,31] Similarly, the variation in the enhanced near field can be achieved either by changing the nanoparticle geometries or by tuning the incident laser waveforms, which can be reflected in the ionization of surface molecules.[15,22,33] When the incident laser intensity increases to approximately 10^{14} W·cm^{-2}, the ionization processes can go into a different regime. In these cases, the generation of large amounts of free electrons and ions can induce dramatic interactions in nanoplasma.[36–38]

In this review, we present an overview of the recent progresses in strong field ionization of molecules on the surface of nanosystems. The emitted ions from surface molecules can be utilized as probes for the near field distributions, and can be further controlled through manipulating the incident laser waveform and manipulating the nanoparticles. The techniques related to laser waveform control and the ion detection are also concluded. The advancements in the field of strong field ionization of molecules on the surface of nanosystems have raised interest in adjustable ion sputtering sources, nanoparticle photocatalysis, etc.

2. Experimental techniques

In this section, we provide an introduction to the manipulation of laser waveforms and the detection techniques for studying the underlying dynamics in nanosystems.

2.1. Manipulation of laser waveforms

The waveforms of the femtosecond laser fields significantly influence the underlying processes induced in various nanosystems. Factors such as wavelength, pulse duration, polarization direction, etc., play crucial roles. Few-cycle laser pulses with well-controlled carrier envelope phase (CEP) and femtosecond two-color laser fields have been utilized to control the ionization processes in nanosystems. For few-cycle laser pulses down almost one optical cycle, manipulation of instantaneous forces acting on bound electrons and influencing their succeeding motion can be achieved by controlling the CEP, where the symmetry of laser waveforms can be dramatically altered accordingly.[19–21] Greater complexity in laser waveform manipulation can be achieved through combining the laser pulses at two different frequencies. This involves coherently superposition of the fundamental wave (FW) and its second harmonics (SH), by precisely tuning the strengths, the polarization directions, and the relative phase of the two components. To give an example, we show two-color femtosecond laser fields combined at various polarizations. The synthesized femtosecond laser fields can be expressed as

$$E_{\text{linear}}(t) = E_{\text{FW}}(t)\cos(\omega_{\text{FW}}t) + E_{\text{SH}}(t)\cos(2\omega_{\text{FW}}t + \phi_{\text{L}}), \quad (1)$$

$$\begin{aligned}\boldsymbol{E}_{\text{bicircular}}(t) = {} & E_{\text{FW}}(t)\left[\cos(\omega_{\text{FW}}t)\boldsymbol{e}_z + \sin(\omega_{\text{FW}}t)\boldsymbol{e}_y\right] \\ & + E_{\text{SH}}(t)\left[\cos(2\omega_{\text{FW}}t + \phi_{\text{L}})\,\boldsymbol{e}_z \right. \\ & \left. \pm \sin(2\omega_{\text{FW}}t + \phi_{\text{L}})\,\boldsymbol{e}_y\right], \end{aligned} \quad (2)$$

where $E_{\text{FW,SH}}(t)$ represent the envelops of the laser fields, ω_{FW} is the frequency of the FW, and ϕ_{L} is the relative phase between the FW and SH. $\boldsymbol{e}_{y,z}$ are the unit vectors along the y and the z directions in the laboratory frame. The linearly polarized two-color fields at various relative phases are presented in Figs. 1(a1)–1(a3). If the two components are linearly polarized at orthogonal directions, the combined laser fields are shown in Figs. 1(b1)–1(b4). Interestingly, if two circular polarized femtosecond laser pulses are used for the superposition, trefoil or semilunar waveforms can be realized, depending on the helicities (Figs. 1(c1)–1(c4) and 1(d1)–1(d4)). For example, a phase-controlled linearly polarized two-color field can be utilized to steer the electrons emitted from dissociative ionization of hydrogen towards recapture by one of the outgoing nuclei.[20] The polarization and relative phase of the two-color laser fields significantly influence selective proton emission during dissociative ionization of molecules absorbed onto SiO_2 nanoparticles.[22]

2.2. Detection techniques

The techniques employed for nanosystems interacting with intense femtosecond laser fields encompass time-of-flight (TOF) spectroscopy, velocity map imaging (VMI) spectroscopy, and reaction nanoscopy. The principle of TOF spectroscopy involves the separation of ions based on their travelling time passing a flight tube.[25] The trajectory of an ion in a TOF spectrometer is determined by its momentum, kinetic energy, acceleration voltage, and m/z ratio. Compared to TOF measurements, experimental results from VMI and reaction nanoscopy can provide more information about angle-resolved momentum and energy distributions. Nano-VMI is developed that combines VMI spectrometer with an aerosol source to study the interactions between femtosecond laser pulses and isolated nanostructures. A simple design of nano-VMI is depicted in Fig. 2. The nanoparticles are delivered into vacuum via an aerosol generator and pass through an aerodynamic lens and a set of skimmers for differential pumping. The application of a flowing aerosol source ensures the availability of fresh nanoparticles for every laser shot, thereby enabling the utilization of single-shot angle-resolved photoion spectroscopy techniques.[23,26,27]

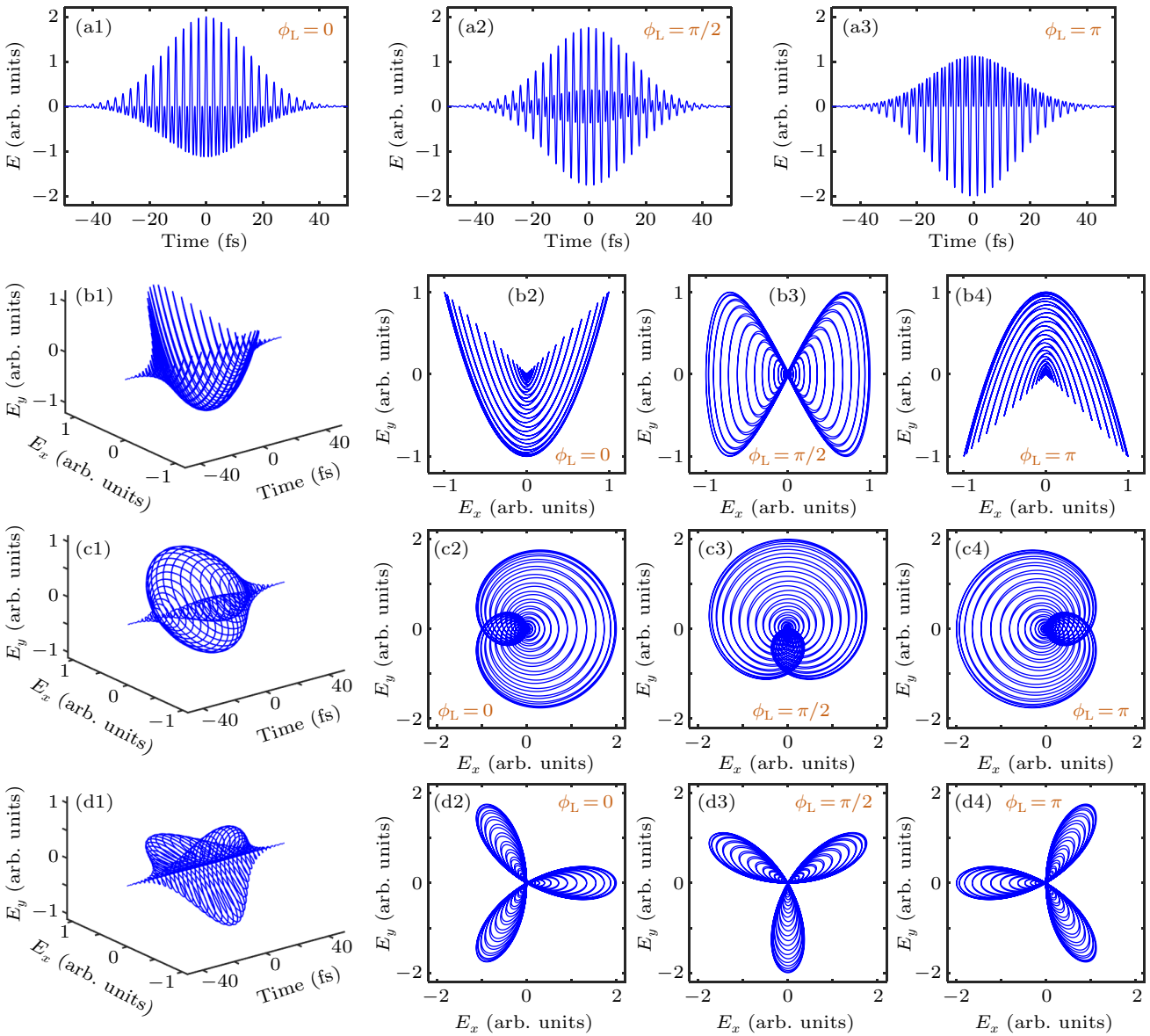


Fig. 1. Waveforms for various two-color femtosecond laser fields. (a1)–(a3) Parallel polarized two-color laser field at $\phi_L = 0, \pi/2, \pi$ ($I_{FW} = I_{SH}$). 3D Waveform and its projection to polarization plane for (b) orthogonal two-color laser field ($I_{FW} = I_{SH}$), (c) corotating two-color laser field, and (d) counter-rotating two-color laser field.

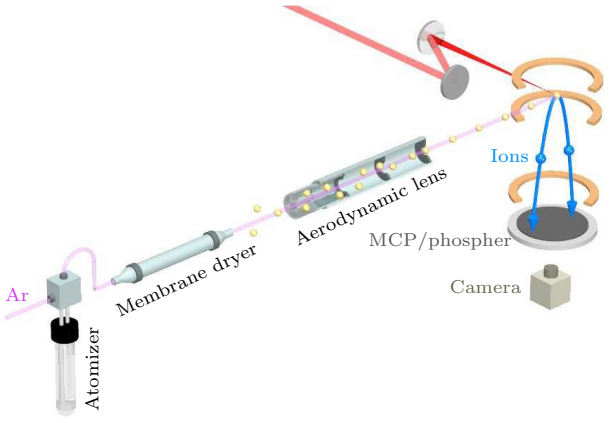


Fig. 2. Schematic diagram of nanoparticle aerosol source and VMI equipment.

The recently developed reaction nanoscopy,[12] which is based on three-dimensional (3D) momentum spectroscopy of charged molecular fragments, enables the imaging of near-field-induced reaction yield distributions on the surface of isolated nanoparticles and their clusters.[28] The experimental setup consists of two side electrode plates, a channeltron for electron counting, microchannel plates (MCP), and a delay-line detector (DLD), as illustrated in Fig. 3. Electrons are accelerated towards the channeltron for precise quantification. Fragments resulting from molecular photodissociation are directed towards the ion detector. In reaction nanoscopy, simultaneous detection of electrons and ions generated from nanoparticle-mediated photoreactions can be achieved. By measuring the time-of-flight and impact positions of ions and electrons on their respective detectors, three-dimensional momentum distributions can be reconstructed to investigate specific reaction processes.

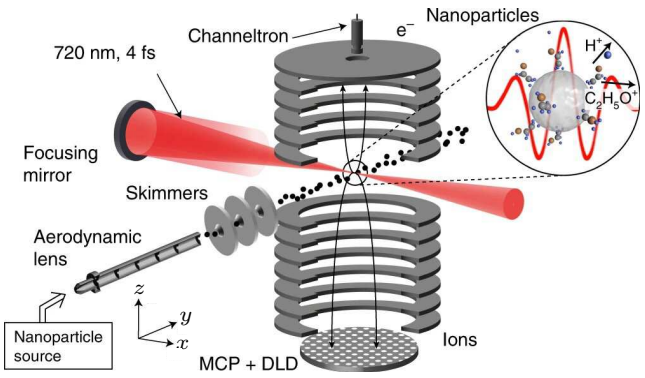


Fig. 3. Schematic drawing of a reaction nanoscope. Fragments arising from molecular photodissociation are accelerated towards the ion detector (bottom: microchannel plates (MCP) and delay-line detector (DLD)) by a homogeneous electric field. Electrons are accelerated towards the opposite side of the spectrometer and are detected with a channeltron (top). Electrons and ions are recorded in coincidence.[12]

3. Surface molecular ionization induced by enhanced near field in nanoparticles

The nanoparticles interacting with intense femtosecond laser fields unavoidably adsorb solvent molecules or radicals on their surfaces. When excited by a femtosecond laser pulse, localized near field will be induced around the nanoparticle. The strength of the induced near field can be somewhat enhanced compared to the incident laser field. This can lead to an efficient near field strength to ionize the surface molecules attached to the nanoparticle when the excitation laser intensity is relatively low. And H^+ ions are the main product of surface ionizations. In recent years, there has been a flourishing research focuses on understanding the ionization mechanisms of surface molecules in nanosystems. The momentum distributions of these ions exhibit intriguing features that reflect the underlying ionization processes occurring. The identification of these ions allows for retrospective identification of the reaction sources. It is worth noting that factors such as the nanoparticle sizes, geometric shapes, and constituents of nanoparticles and the solvents play crucial roles in determining both the near-field effects and the ionization processes.

3.1. Ion emission from isolated nanoparticles in well-controlled femtosecond laser fields

Dielectric materials, due to the absence of loosely bound or free electrons drifting through the material, undergo polarization when exposed to an electric field. This results in moving towards the outer direction for the positive charges and moving in the opposite direction for the negative charges, thereby generating a robust internal field that diminishes the overall electric field within the material. Simultaneously, the light-and-nanoparticle interaction significantly amplifies the electric field on the nanoparticle surface, leading to a plethora of intriguing phenomena. Within the region of relatively low laser intensities, the momentum distributions of ions emitted from a single nanoparticle are predominantly determined by the localized near-fields, which are closely dependent upon the driving laser fields.

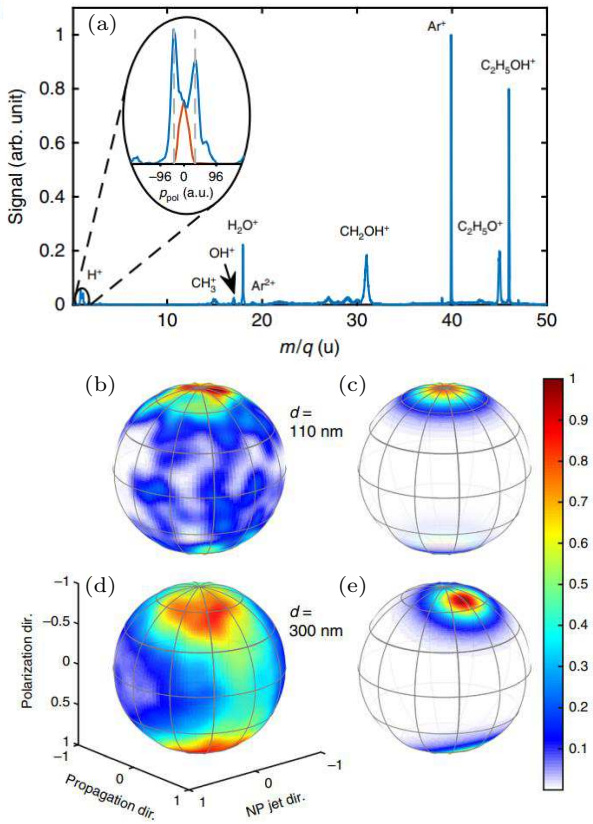


Fig. 4. (a) Averaged time-of-flight spectrum from SiO_2 nanoparticles exposed in intense femtosecond laser fields. The inset figure shows the enlarged peak of H^+ ions on a momentum scale along the polarization direction (p_{pol}), for events with nanoparticles (blue) and with just background gas (red). (b)–(e) Comparison of the measured and calculated proton distributions. The 3D (φ, θ, r) momentum distributions of protons are integrated along the radial coordinate and the retrieved two-dimensional (φ, θ) density map is spanned over a unit sphere. The number of protons per solid angle is encoded in the color scale. (b) Measured and (c) calculated proton distributions for the 110 nm particles. (d) Measured and (e) calculated proton distributions for the 300 nm particles.[12]

The formation of complicated elements in aerosol nanoparticles, originating from the nanoparticles, the residual solvents and the background gases, determines the variety of ions that will be emitted from the laser focusing region. Figures 4(b)–4(e) illustrate the angular momentum of protons ejected from SiO_2 nanoparticles with diameters of $d = 110$ nm and $d = 300$ nm.[12] When the particle diameter (110 nm) is much smaller than the laser wavelength (720 nm), the momentum distribution of protons exhibits a dipole shape. This characteristic can be attributed to the electrostatic field generated by charged nanoparticles, which repels protons while neglecting fast escaping electrons. To provide a clear explanation, we introduce Mie parameter $\rho = \pi d/\lambda$,[30] where d represents the diameter of the nanosphere and λ denotes the excitation wavelength. When $\rho \ll 1$, the localized near-field exhibits a dipole shape that drives protons to form a similarly shaped momentum distribution as dictated by electrostatic field properties.

When the diameter is increased to a level such that $\rho \sim 1$, e.g., $d = 300$ nm, the localized near-field exhibits a focusing effect, resulting in the forward bending in the proton momentum distribution. In a word, the distribution of the enhanced near-field on nanoparticle surface significantly influences the proton ejection behavior.

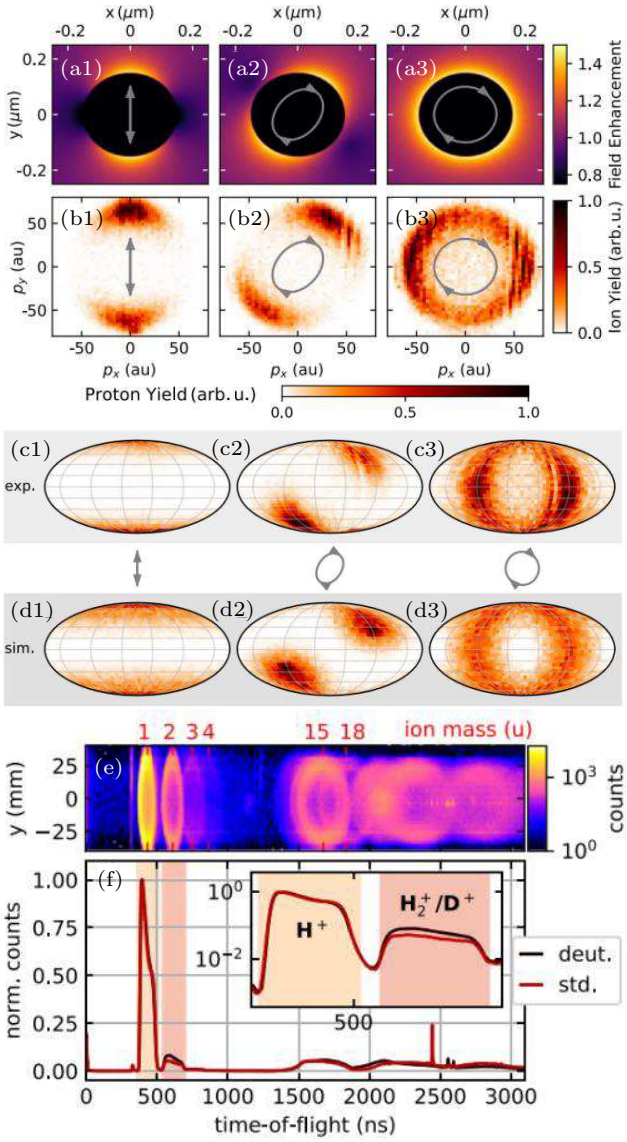


Fig. 5. (a) The enhanced near field distributions and (b) the projected proton momentum distributions on the polarization plane for 300 nm silica nanoparticles. (c) The experimental data and (d) the simulation of mollweide projection of the angular distributions of the proton yield. The gray symbols indicate the polarization state for each panel. The pulse energy is 18 μJ in all cases, corresponding to a peak intensity at about 2×10^{13} W·cm^{-2} for the linearly polarized case. The numbers 1, 2, 3 in panels (a)–(d) represent the results for linear (waveplate angle: 0°), elliptic (waveplate angle: 35°), and circular (waveplate angle: 45°) polarizations, respectively. (e) Histogram as a function of position and time-of-flight for 300 nm silica nanoparticles in (fully deuterated) methanol-d4 excited by circular polarized laser pulses. (f) Time-of-flight spectra of ions emitted from 300 nm silica nanoparticles.[15]

When exposed to elliptically polarized laser fields, the overall distributions of field enhancement and thus the proton momentum distributions in the polarization plane exhibit similar shapes. However, there are variations in localized field magnitudes as depicted in Figs. 5(a1)–5(a3) and 5(b1)–5(b3).[15] To confirm that protons originate from dissociative ionization of hydroxyl radicals from covalently bound silanol groups, experiments by replacing the solvent with methanol and fully deuterated methanol-d4 have been conducted. Remarkably, even with these changes, protons still dominate the TOF spectrum (Fig. 5(f)), showing nice agreement between the experimental (Figs. 5(c1)–5(c3)) and the calculated results (Figs. 5(d1)–5(d3)). This suggests that any residual solvent on nanoparticles rapidly evaporates upon injection into a vacuum environment, thereby the detected protons primarily arise from covalently bound silanol groups.

With the advancement of experimental and theoretical investigations on near-field induced ionization of nanoparticles, there is an anticipation for further realization of complex polarization and waveform control. Boris Bergues *et al.*[22] have reported the achievement of all-optical control over the proton emission in nanoparticles. By analyzing the ion momentum distribution in the polarization plane, it is observed that SiO_2 nanoparticles with diameter of ~ 300 nm interacting with linearly polarized two-color laser pulses (comprising an FW at 2 μm and an SH component at 1 μm) can generate asymmetric near-field when the relative phase ϕ_L is either 0 or π, resulting in either upward or downward proton emissions (Figs. 6(b1)–6(b4)). These findings are consistent with the calculated near field distributions obtained from FDTD simulations (Figs. 6(a1) and 6(a2)). Furthermore, the proton emission depends on ϕ_L while exhibiting weak depends on the emission energy. Hence, the regulation of one-dimensional proton emission can be achieved through precise adjustment of the relative phase of the two-color laser fields. The phase-dependent angular distribution Θ_f^{xy} of protons ejecting from 300 nm and 600 nm nanoparticles shows similar oscillation in the ion yield but different in the most probable emission at angles of about $\pm 90°$ and $\pm 70°$ (Figs. 6(c1)–6(c4)).

When excited using bicircular two-color laser pulses, more complex manipulation of the proton emission can be achieved. Figures 6(d) and 6(e) show the momentum distributions and the asymmetry maps of protons at $\phi_L = 0$ and $\phi_L = \pi$. In the counter-rotating condition, three maximum regions can be obtained for the whole angular range (Figs. 6(d1)–6(d4)), whereas in the co-rotating condition, only one lobe is observed (Figs. 6(e1)–6(e4)), agreeing with the calculated results depicted in Figs. 6(a3)–6(a6). However, it should be noted that the maximum asymmetry value of protons for the counter-rotating condition ($\sim 75\%$) is considerably lower compared to that of co-rotating cases ($\sim 30\%$). Consequently, by tailoring the laser waveforms, the nanoscale near field distributions and charge distributions on the surface of nanoparticles can be well controlled thus influencing the directional proton ejections.

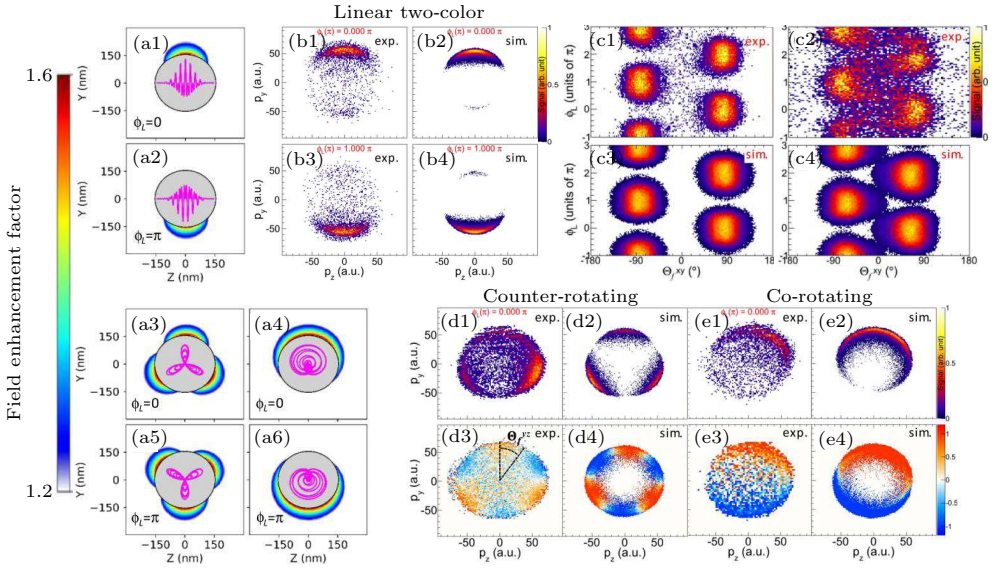


Fig. 6. The enhanced near field distributions for 300 nm SiO_2 nanoparticle exposed to ((a1), (a2)) linear, ((a3), (a5)) counter-rotating and ((a4), (a6)) co-rotating bicircular two-color laser fields. Proton momentum distribution from ((b1), (b3)) experiments and ((b2), (b4)) simulations on 300 nm SiO_2 nanoparticles exposed to phase-changed linear two-color laser fields. (c1) Measured and (c3) simulated emission angle Θ_f^{xy} and phase ϕ_L-resolved momentum distributions of protons from 300 nm SiO_2 nanoparticles in linearly polarized two-color laser fields. Panels (c2) and (c4) are same as panels (c1) and (c3) but for the case of 600 nm nanoparticle. (d1) Measured and (d2) simulated momentum distributions of protons emission at $\phi_L = 0$ of a counter-rotating bicircular two-color pulse. (d3) and (d4) The corresponding two-dimensional asymmetry pattern of the spatially selective proton emission. Panel (e) is same as panel (d) but for the case of co-rotating bicircular two-color pulse.[22] Adapted with permission from Ref. [22] © Optical Society of America

3.2. Forward focusing effect in surface molecular ionization for nanoparticle dimers

When using the aerosol source, there are inevitably a certain amount of nanoparticle dimers in the floating nanoparticles towards the interaction region. FDTD calculations indicate that the degree of field enhancement is apparently larger in dimer systems compared to isolated particles (as shown in Fig. 7(a)), therefore surface ionization from nanoparticle dimers can dominate the reactions especially for relatively low laser intensities. It has been demonstrated that protons emitted from surface molecules on nanoparticles can serve as probes for detecting the spatial distributions of dissociative ionization yields.[31] Nanoparticle clusters consisting of only a few silica nanoparticles can be transmitted to the vacuum through the aerosol source. The formation probability of nanoparticle dimers increases for higher particle concentrations in the aqueous suspension. As the dimer injection increases, proton yield in the forward direction gradually becomes dominant (Figs. 7(b)–7(d)), which can be dominated by the localized near fields (Fig. 7(a)). By analyzing the momentum distributions obtained from nanoparticle flow generated from high concentration solutions, as shown in Fig. 7(e), events originating from single nanoparticles can be identified due to their dipole-shaped momentum distributions. Therefore, at relatively lower laser intensities (around 1.5×10^{13} W·cm^{-2}), protons are mainly produced from nanoparticle dimers rather than individual nanoparticles.

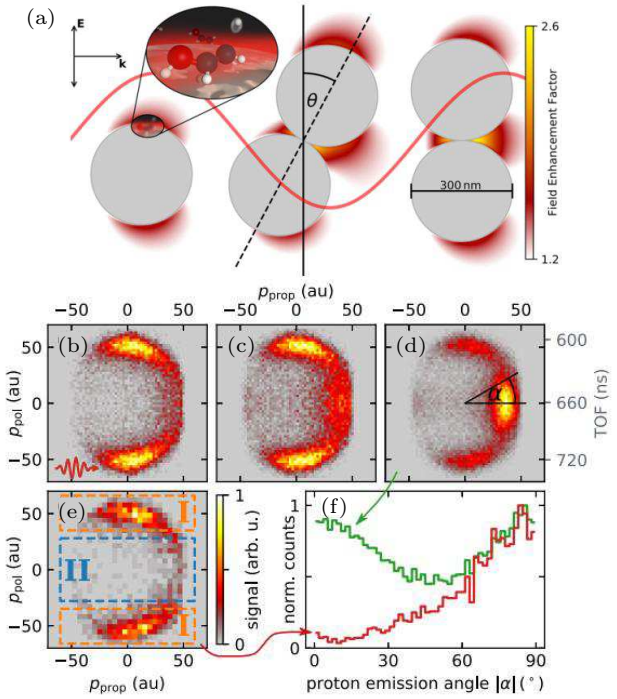


Fig. 7. (a) Near-field distributions in the polarization–propagation plane for a 300 nm silica nanosphere and its dimers. Measured proton momentum distributions for different sample concentrations. (b)–(d) Proton momentum distributions, in atomic units (a.u.), in the polarization–propagation plane for dispersed silica nanoparticle concentrations of 0.2 g/L, 0.4 g/L and 1.5 g/L, respectively. The data are taken at a peak intensity of 5×10^{13} W·cm^{-2}. (e) Events from the data in panel (d) reduced to two coincidently detected protons per laser shot. (f) Angular distributions of counts for the data from panel (d) green line and panel (e) red line, where the definition of the proton emission angle α is contained in panel (d).[31] Reprinted (adapted) with permission from (COMPLETE REFERENCE CITATION). Copyright (2020) American Chemical Society.

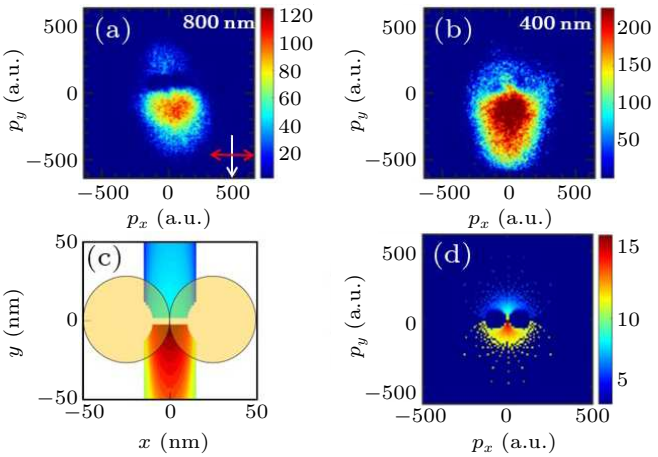


Fig. 8. The single-shot momentum distributions for the ions ejected from the nanoparticle systems. The black and red arrows indicate the laser propagation and polarization directions, respectively. Panels (a) and (b) are the momentum distributions for the Si^+ ions at an excitation intensity of about 3×10^{13} W·cm^{-2}. Panels (c) and (d) are the calculated initial charge distributions and the final momentum distributions.

Not only do the ion products from surface molecules exhibit forward focusing effect in the dimer system, but also the ions generated from the nanoparticles display a distinct forward focusing momentum distribution from nanoparticle dimers.[24] At the laser intensities from 1.7×10^{13} W·cm^{-2} to 3×10^{13} W·cm^{-2}, the ejected Si^+ ions from SiO_2 nanoparticle dimers show a clear forward distribution, as being presented in Figs. 8(a) and 8(b). In order to elucidate the hollow core structure observed in the momentum distribution of Si^+, a two-dimensional simulation (Figs. 8(c) and 8(d)) employing Newtonian equations involving Coulomb interactions is employed. Calculations demonstrate that this specific momentum distributions are originated from Coulomb repulsion within spatially separated charges in nanoparticle dimers.

3.3. Orientation-dependent ion emission originated from near-field deformation in nanosystems

With the development of material science and nanofabrication techniques, novel nanostructures can be designed and produced, providing endless potential for manipulation of the light-and-nanostructure interactions. The near field induced in various nanosystems, e.g., in nanotubes and nanocubes, exhibits variations in relation to the spatial alignment between the axis of symmetry and the polarization direction of the laser fields. This leads to orientation dependent ion emissions.[32]

Nanoparticles composed of metal materials possess the ability to shield electric fields within. The reaction of a gold nanocube in intense femtosecond laser field has been studied by detecting the ion products from surface molecular ionization.[33] To calculate the near-field distribution surrounding a nanocube, a discontinuous Galerkin time-domain (DGTD) method is utilized. When compared to similarly sized nanospheres, nanocubes exhibit distinct orientation dependence in the near field distribution and more pronounced propagation effects, as depicted in Fig. 9. At relatively low laser intensities, the final momentum distribution of the ejected ions is primarily determined by the initial charge distribution that was induced by the enhanced near field. As a result, protons emitted from the surface of nanoparticles can serve as probes to detect the instantaneous near-field distribution. Since the size of the laser focus is significantly larger than that of nanoparticles, each nanoparticle may experience varying laser intensities, resulting in proton momentum distributions with distinct characteristics. By sorting the total number of protons in each frame, a histogram can be derived corresponding to grouped events with increasing light intensity.

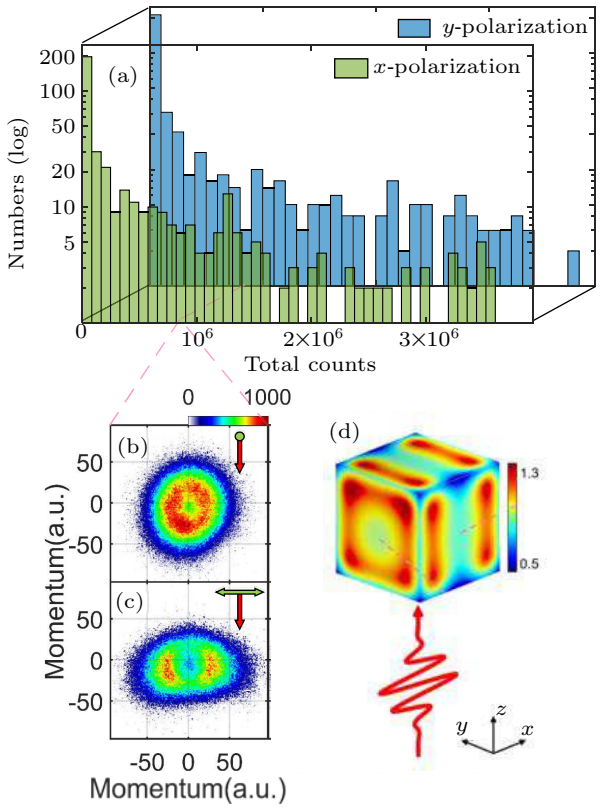


Fig. 9. (a) Histograms obtained for the H^+ ions at x- and y-polarization excitations. (b) Momentum distribution obtained by integrating the single-shot images within three distinct histogram regions for the y-polarization, corresponding to different intensity conditions. The red and green arrows indicate the laser propagation and polarization directions, respectively. Panel (c) is same to panel (b) but for the x-polarization. (d) The DGTD simulation result of the near field distribution at the surface of a gold nanocube (90 nm) in the exciting laser whose wavelength is 800 nm.[33] Adapted with permission from Ref. [33] © Optical Society of America

3.4. Nanocluster and mosaic nanostructure

Nanoparticles with irregular shapes also possess interesting features when excited with femtosecond laser pulses. For instance, 100 nm TiO_2 nanoclusters composed of $\sim$ 5 nm crystals are utilized to investigate the motion of ionized particles.[29] Compared to NaCl nanocrystals with similar dimensions, the ejection of ions from TiO_2 nanoclusters exhibits a roughly symmetric distribution, as depicted in Figs. 10(a) and 10(b). FDTD results validate that the field strength sur-

rounding an individual TiO_2 nanocrystal is significantly enhanced on its surface. However, there is no preferential direction for laser propagation when it comes to clusters.

Another experiment is conducted with a 50 nm Au nanoparticle embedded on a 100 nm poly-vinylpyrrolidone (PVP) sphere, compared with multiple 17 nm Au nanoparticles embedded on PVP nanosphere.[29] Considering that the Au nanostructure embedded on the surface might be ionized prior to the PVP, the laser field can be strongly absorbed near the surface of the Au nanoparticle, leading to the formation of localized nanoplasma. The experimental results demonstrate that the directions of ion explosion for the 50 nm Au-PVP combination are equally probable in all orientations in multiple measurements. Molecules around the Au sphere dominate ionization process, and the Au sphere orientation is random. Thus confirming that spatial orientation of nanostructures serves as a determining factor. In 17 nm Au-PVP hybrid structures, the ions predominantly emit in the direction opposite to the propagation direction. This discrepancy can be attributed to plasma generation occurring primarily within the gaps between Au nanoparticles, where localized field enhancement is significant. It appears that laser penetration depth can be impeded by the adhesive Au nanoparticles.

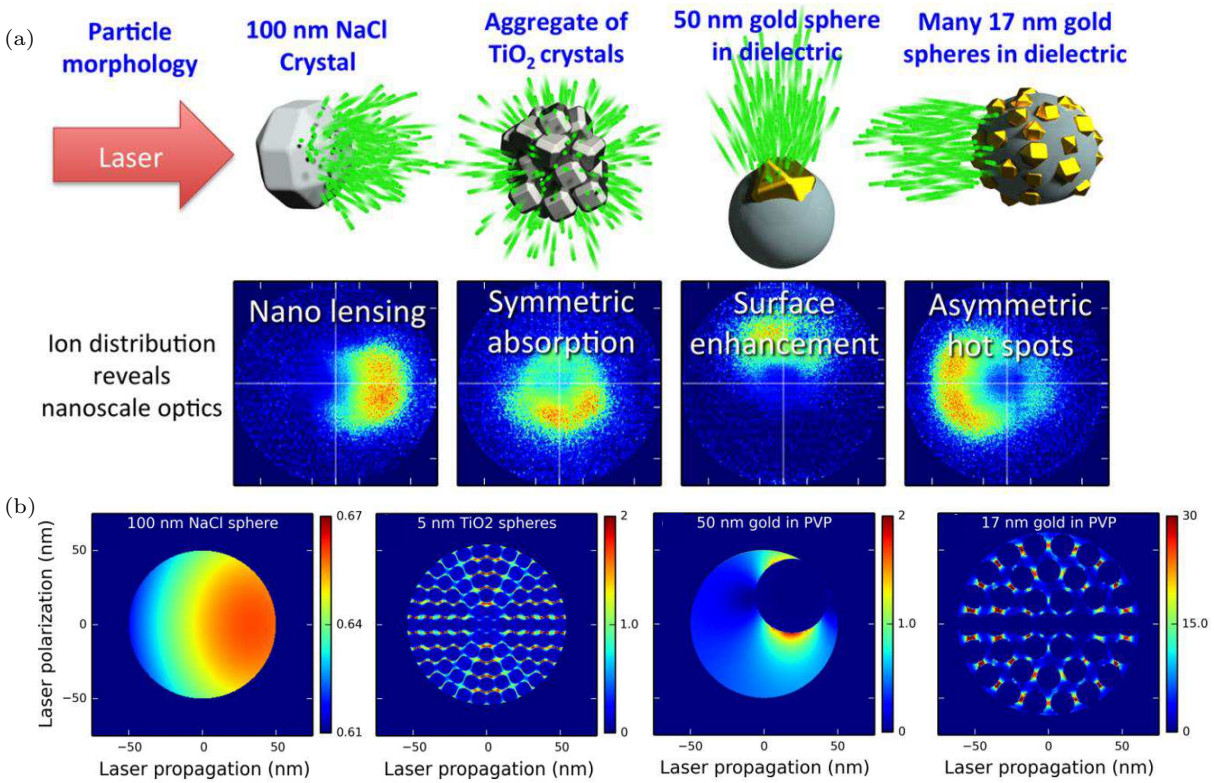


Fig. 10. (a) Nanoscale light absorption mechanisms and (b) FDTD calculations of the electric field intensity inside the various nanostructures with similar diameter ($\sim$ 100 nm), including NaCl particles, TiO_2 aggregates, 50-nm-gold-PVP nanostructures and structures composed of 17 nm gold nanospheres and PVP. The laser propagates from left to right, and the color scale is in units of the incident field intensity.[29]

3.5. Surface molecular ionizations in nanodroplets

Investigations have also been carried out on surface ionizations in nanodroplets.[28] The resulting ion emission can be utilized for molecular structure analysis on the surface of propanediol (PDO) nanodroplets, including 1,2-PDO and 1,3-PDO. The intensity-dependent proton momentum distributions reveal that the dominance of the dipole component increases with laser intensity, which can be attributed to the nanoparticle size effect.[18] Simultaneously, the most probable emission angle α_{max} (with respect to propagation direction) approaches 90° and correlates with droplet size which can be reproduced by calculations using Mie-solution of Maxwell's equation.[30,35] Unlike solid nanoparticles, nanodroplets tend to rupture when they contain an excessive number of charges beyond the Rayleigh limit.[34] In a droplet environment, variations in CH_3^+ yield between 1,2-PDO and 1,3-PDO can be attributed to distinct molecular arrangements on the droplet surface.

4. Ion shock wave formation in nanoparticles

When the excitation laser intensities reach approximately 10^{14} W·cm^{-2}, the dramatic ionizations in nanosystems can produce sufficient charged particles thus forming nanoplasma. The ionized electrons can be subsequently accelerated by the strong laser field and undergo impact ionization, leading to high temperatures.[36–38] By exposing the nanocrystals of NaCl, KCl, KI, and NH_4NO_3 ($\sim$ 100 nm) to dual laser pulses (at 400 nm and 800 nm, respectively) with adjustable delay,

people reported a sharp ring structure in the two-dimensional projection of the photoion angular distribution (PAD), i.e., the shock wave formation, as depicted in Fig. 11(a).[23] The threshold laser intensity required to induce shock formation is approximately proportional to the ionization potential of the compound. Notably, NH_4NO_3 nanoparticles possess a high ionization potential and do not produce shock waves in a single pulse excitation condition, making them suitable for dual laser experiments. It is demonstrated that the formation of shock waves strongly relies on the timing between pulses. The first pulse excites the nanostructure to generate an expanding nanoplasma, while the second arriving pulse ignites the shock wave. To produce a shock wave in nanoplasma, the strengths and the relative time delay of the two excitation laser pulses need to be optimized.[39,40] When the electron density of the plasma reaches the critical level, resonant interaction between the laser field and electrons can cause enhancement in energy absorption. It has been demonstrated that the increase in ionization yield occurs on a timescale similar to shock wave formation, confirming that both processes rely on plasma expansion dynamics. Moreover, it is important to note that the time delay also influences the probability of shock wave formation.

Shock wave formations can also be achieved with single pulse excitation. Clear shock wave structures have been obtained in the H^+ and Si^+ ions emitted from 50 nm SiO_2 nanospheres excited with single femtosecond pulse, as shown in Figs. 11(b) and 11(c).[24] In this study, the shock waves have been discovered both in the surface ion emission and in the ion product distributions of the nanoparticle. Compared to the sharp rings observed for the H^+ ions, the Si^+ shock waves exhibit a broader radial momentum distribution ranging towards $\sim$ 500 a.u. The different features observed for the surface molecular ionization product and the Si^+ ions produced from the nanoparticle may be attributed to the fact that the Si^+ ions could be emitted from different depths in the nanoparticles thus producing a broad distribution in momentum. As high-velocity inner ions surpass their lower-velocity outer counterparts, a critical surface characterized by high charge densities is formed, thereby forming the ion shock waves.

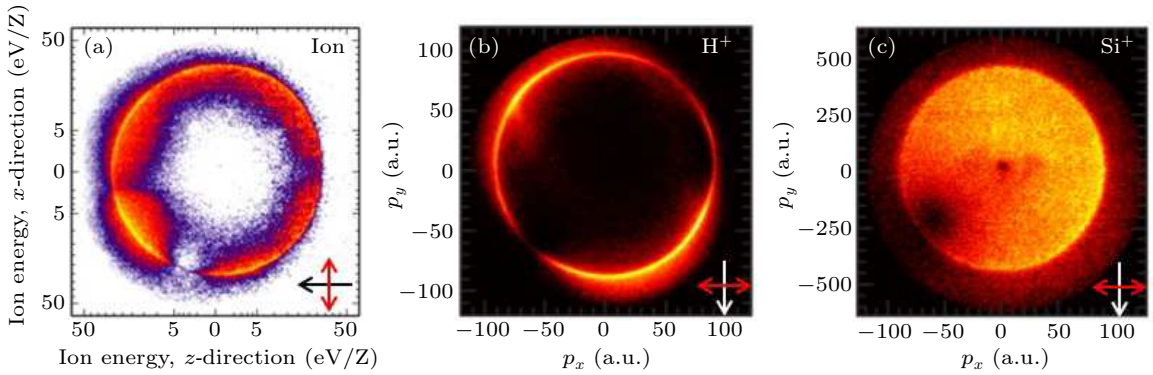


Fig. 11. (a) The sharp photoion angular distribution (PAD) of shock wave from a single NH_4NO_3 nanoparticle irradiated with dual femtosecond laser pulses at 400 nm and 800 nm. The black and red arrows indicate the laser propagation and polarization directions, respectively.[23] (b) The momentum distribution of the H^+ ions from a single SiO_2 nanoparticle irradiated with a single beam of laser pulses at 800 nm, showing shock wave features. Panel (c) is similar to panel (b) but is obtained for the Si^+ ions. The white and red arrows indicate the laser propagation and polarization directions, respectively.

5. Conclusion

We introduce some of the important results in the surface molecular ionizations in nanosystems excited by tailored femtosecond laser fields. The interaction between nanoparticles and femtosecond laser fields leads to a non-uniform enhancement in the localized electric fields in the close vicinity to the nanoparticles, therefore dominating the ionizations of molecules attached to the surface. By manipulating the laser waveforms and altering nanoparticle appearances, it becomes possible to control and direct the characteristic ion emissions from surface molecular ionizations. At relatively low laser intensities, the momentum distribution of surface ions emitted from individual nanoparticles predominantly exhibits a feature reflecting the near field distribution. As the incident laser intensity increases, more and more charged particles can be produced in the light and nanoparticle interactions thus can generate a nanoplasma, where dramatic absorption and ionization processes occur. The exploration of related underlying dynamics is still lacking. Advanced experimental techniques for studying the surface ionization processes have been developed in recent years to explore the unknown phenomena. However, the strong field and nanoparticle interactions discussed in this review are manybody systems comprising a substantial number of electrons and ions. The interaction between many particles in strong laser fields gives rise to complex dynamics that pose great challenges for theoretical calculations. At high laser intensities, existing theoretical models become inadequate in explaining the underlying dynamics in the nanometer and femtosecond spatial temporal regime. The blooming experimental observations can definitely help to establish new models to study the nanosystems. We expect the

development of advanced experimental and theoretical efforts in the field and more significant investigations taken place for revealing the mysterious physical mechanisms. These are of great importance for further precise control of the light-and-matter interactions at the extreme spatial temporal levels.

Acknowledgment

Project supported by the National Natural Science Foundation of China (Grant Nos. 92050105, 92250301, and 12227807).

References

[1] Brabec T and Krausz F 2000 *Rev. Mod. Phys.* **72** 545
[2] Becker W, Grasbon F, Kopold R, Milošević D B, Paulus G G and Walther H 2002 *Adv. At. Mol. Opt. Phys.* **48** 35
[3] Scrinzi A, Ivanov M Y, Kienberger R and Villeneuve D M 2006 *J. Phys. B: At. Mol. Opt. Phys.* **39** R1
[4] Milošević D B, Paulus G G, Bauer D and Becker W 2006 *J. Phys. B: At. Mol. Opt. Phys.* **39** R203
[5] Krausz F and Ivanov M 2009 *Rev. Mod. Phys.* **81** 163
[6] Lewenstein M, Balcou P, Ivanov M Y, L'Huillier A and Corkum P B 1994 *Phys. Rev. A* **49** 2117
[7] Corkum P B 1993 *Phys. Rev. Lett.* **71** 1994
[8] Krausz F and Stockman M I 2014 *Nat. Photonics* **8** 205
[9] Schoetz J, Wang Z, Pisanty E, Lewenstein M, Kling M F and Ciappina M F 2019 *ACS Photonics* **6** 3057
[10] Thomas S, Wachter G, Lemell C, Burgdörfer J and Hommelhoff P 2015 *New J. Phys.* **17** 063010
[11] Kim S, Jin J, Kim Y J, Park I Y, Kim Y and Kim S W 2008 *Nature* **453** 757
[12] Rupp P, Burger C, Kling N G, Kübel M, Mitra S, Rosenberger P, Weatherby T, Saito N, Itatani J, Alnaser A S, Raschke M B, Rühl E, Schlander A, Gallei M, Seiffert L, Fennel T, Bergues B and Kling M F 2019 *Nat. Commun.* **10** 4655
[13] Rupp P, Seiffert L, Liu Q, Süßmann F, Ahn B, Förg B, Schäfer C G, Gallei M, Mondes V, Kessel A, Trushin S, Graf C, Rühl E, Lee J, Kim M S, Kim D E, Fennel T, Kling M F and Zherebtsov S 2017 *J. Mod. Opt.* **64** 995
[14] Liu Q, Seiffert L, Süßmann F, Zherebtsov S, Passig J, Kessel A, Trushin S A, Kling N G, Ben-Itzhak I, Mondes V, Graf C, Rühl E, Veisz L, Karsch S, Rodríguez-Fernández J, Stockman M I, Tiggesbäumker J, Meiwes-Broer K H, Fennel T and Kling M F 2020 *ACS Photonics* **7** 3207
[15] Rosenberger P, Dagar R, Zhang W, Sousa-Castillo A, Neuhaus M, Cortes E, Maier S A, Costa-Vera C, Kling M F and Bergues B 2022 *Eur. Phys. J. D* **76** 109
[16] Salditt T, Egner A and Luke D R 2020 *Nanoscale Photonic Imaging* (Cham: Springer) p. 523
[17] Powell J A, Summers A M, Liu Q, Robatjazi S J, Rupp P, Stierle J, Trallero-Herrero C, Kling M F and Rudenko A 2019 *Opt. Express* **27** 27124
[18] Seiffert L, Süßmann F, Zherebtsov S, Rupp P, Peltz C, Rühl E, Kling M F and Fennel T 2016 *Appl. Phys. B* **122** 101
[19] Li H, Gong X, Lin K, De Vivie-Riedle R, Tong X M, Wu J and Kling M F 2017 *J. Phys. B: At. Mol. Opt. Phys.* **50** 172001
[20] Zhang W, Yu Z, Gong X, Wang J, Lu P, Li H, Song Q, Ji Q, Lin K, Ma J, Li H, Sun F, Qiang J, Zeng H, He F and Wu J 2017 *Phys. Rev. Lett.* **119** 253202
[21] Zhang W, Li H, Gong X, Lu P, Song Q, Ji Q, Lin K, Ma J, Li H, Sun F, Qiang J, Zeng H and Wu J 2018 *Phys. Rev. A* **98** 013419
[22] Zhang W, Dagar R, Rosenberger P, Sousa-Castillo A, Neuhaus M, Li W, Khan S A, Alnaser A S, Cortes E, Maier S A, Costa-Vera C, Kling M F and Bergues B 2022 *Optica* **9** 551
[23] Hickstein D D, Dollar F, Gaffney J A, Foord M E, Petrov G M, Palm B B, Keister K E, Ellis J L, Ding C, Libby S B, Jimenez J L, Kapteyn H C, Murnane M M and Xiong W 2014 *Phys. Rev. Lett.* **112** 115004
[24] Sun F, Li H, Song S, Chen F, Wang J, Qu Q, Lu C, Ni H, Wu B, Xu H and Wu J 2021 *Nanophotonics* **10** 2651
[25] Greaves J and Roboz J 2013 *Mass Spectrometry for the Novice* (Boca Raton: Taylor & Francis Group) p. 42
[26] Eppink A T J B and Parker D H 1997 *Rev. Sci. Instrum.* **68** 3477
[27] Hickstein D D, Ranitovic P, Witte S, Tong X M, Huismans Y, Arpin P, Zhou X, Keister K E, Hogle C W, Zhang B, Ding C, Johnsson P, Toshima N, Vrakking M J J, Murnane M M and Kapteyn H C 2012 *Phys. Rev. Lett.* **109** 073004
[28] Rosenberger P, Dagar R, Zhang W, Majumdar A, Neuhaus M, Ihme M, Bergues B and Kling M F 2023 *Nanophotonics* **12** 1823
[29] Hickstein D D, Dollar F, Ellis J L, Schnitzenbaumer K J, Keister K E, Petrov G M, Ding C, Palm B B, Gaffney J A, Foord M E, Libby S B, Dukovic G, Jimenez J L, Kapteyn H C, Murnane M M and Xiong W 2014 *ACS Nano* **8** 8810
[30] Mie G 1908 *Ann. Phys.* **330** 377
[31] Rosenberger P, Rupp P, Ali R, Alghabra M S, Sun S, Mitra S, Khan S A, Dagar R, Kim V, Iqbal M, Schötz J, Liu Q, Sundaram S K, Kredel J, Gallei M, Costa-Vera C, Bergues B, Alnaser A S and Kling M F 2020 *ACS Photonics* **7** 1885
[32] Han X, Huang H, Huang X, Cao W, Zhang Q and Lu P 2023 *Adv. Opt. Mater.* **11** 2201260
[33] Wang J, Qu Q, Sun F, Song S, Gao J, Wu B, Xu H, Li H and Wu J 2023 *Opt. Express* **31** 9678
[34] Rayleigh F R S L 1882 *Lond. Edinb. Dublin Philos. Mag. J. Sci.* **14** 184
[35] Bohren C F and Huffman D R 1998 *Absorption and Scattering of Light by Small Particles* (New York: John Wiley & Sons) p. 82
[36] Ditmire T, Donnelly T, Rubenchik A M, Falcone R W and Perry M D 1996 *Phys. Rev. A* **53** 3379
[37] Ammosov M V, Delone N B and Krainov V 1986 *Proceedings of the* 1986 *Quebec Symposium*, June 3–6, 1986, Quebec, Canada, p. 0664
[38] Döppner T, Müller J P, Przystawik A, Göde S, Tiggesbäumker J, Meiwes-Broer K H, Varin C, Ramunno L, Brabec T and Fennel T 2010 *Phys. Rev. Lett.* **105** 053401
[39] Döppner T, Fennel T, Diederich T, Tiggesbäumker J and Meiwes-Broer K H 2005 *Phys. Rev. Lett.* **94** 013401
[40] Döppner T, Fennel T, Radcliffe P, Tiggesbäumker J and Meiwes-Broer K H 2006 *Phys. Rev. A* **73** 031202